sciendo
10.2478/jlecol-2022-0007 Journal of Landscape Ecology (2022), **Vol: 15 / No. 1.**

MODELING AND MAPPING OF SOIL WATER EROSION RISKS IN THE SROU BASIN (MIDDLE ATLAS, MOROCCO) USING THE EPM MODEL, GIS AND MAGNETIC SUSCEPTIBILITY

HASSAN MOSAID[1], AHMED BARAKAT[1]*, VINCENT BUSTILLO[2,3], JAMILA RAIS[1]

[1]Georesources and Environment Team, Faculty of Sciences et Techniques, Sultan Moulay Slimane University, Morocco.
[2] CESBIO, University of Toulouse, CNES/CNRS/INRAE/IRD/UPS, Toulouse, France.
[3] IUT Paul Sabatier, Site d'Auch, France.
**Corresponding author email: a.barakat@usms.ma*

Received: 9th February 2022, **Accepted:** 12th April 2022

ABSTRACT

The Oued Srou watershed located in the Middle Atlas Mountain of Morocco has been a subject of serious soil erosion problems due to the combination of natural factors and anthropic activities. Therefore, soil erosion hazard assessment and mapping can be handy to initiate remedial measures in the area. In this study, the improved Erosion Potential Model (EPM) integrated with GIS and remote sensing techniques is employed to map and assess the vulnerability of the Oued Srou watershed to the water erosion phenomenon and its impact on the silting of the Ahmed El Hansali dam. The results of the EPM model showed that the maximum annual soil loss rates were in the range of 5-652 m^3/km^2/year, with an average of 49 m^3/km^2/year. The delivery coefficient ratio showed that about 34433 t/year of the sediments reach the outlet of the watershed. The correlation analysis between all erosion factors revealed the following order of their importance in the water erosion control: soil sensitivity to erosion, soil protection, slope, erosive state, temperature, and rainfall. The magnetic susceptibility provided results on the evolution of soils; it showed that the most degraded soils had a high erosion rate. Generally, the stable soils not eroded showed an upward increase of magnetic susceptibility values in soil profiles; the evolution of magnetic susceptibility of degraded soils is disturbed. The magnetic susceptibility has also made it possible to highlight the source zones of sediments that reach the outlet of the watershed.

Keywords: Soil erosion, Erosion potential method, Magnetic susceptibility, GIS, Srou River

INTRODUCTION

Soil erosion is a great environmental concern in the world because it negatively affects natural resources and threatens the sustainable development of human society (Lal, 2003; Rozos *et al.*, 2013). Soil erosion, the first major form of soil degradation, is exacerbated by the dynamic activity of erosive agents like water and wind and human activities such as agricultural activities. It can occur as different types of erosion, including interrill, sheet, rill, gully, and stream erosions (Martín-Moreno *et al.*, 2016). Besides this problem of land

degradation, the redistribution of soil particles by water has other off-site problems related to the reduction of crop productivity, such as corn loss (Lal *et al.*, 1999; Duan *et al.*, 2016; Novara *et al.*, 2018; Plambeck, 2020), deterioration of water quality (Sthiannopkao *et al*., 2007; Issaka & Ashraf, 2017; Hou *et al*., 2020), and silting of lakes (Rãdoane &Rãdoane, 2005; Wang *et al*., 2014; Borrelli *et al*., 2020). So, assessing soil erosion and its risk is essential for planning and implementing soil conservation measures. Hence, assessing soil erosion and its risk is necessary for further watershed management planning and operation of soil and water protection actions. Therefore, soil erosion studies have been increasing during the past few decades (El Jazouli *et al*., 2019b; Panagos & Katsoyiannis, 2019; Fang & Fan, 2020; Luetzenburg *et al*., 2020) due to the great extent of soil erosion.

Furthermore, many techniques and models have been developed to assess the hydric soil loss in terms of rate and frequency (de Jong *et al*., 1998; Walling & He, 1999; Kinnell, 2017; Batista et al. 2019; Ketema and Dwarakish 2019; Mohammed et al. 2020; Mosavi et al. 2020; Senanayake *et al*., 2020). Besides the expensive field survey methods, numerous mathematical models have been developed worldwide to assess soil erosion. This diversity in models is linked to the complexity of factors (precipitation, topography, soil properties, land use/land cover (LULC) dynamics) controlling soil erosion and their variability in time and space. These models developed for estimating the sediment yield from watersheds are generally classified as empirical, conceptual, and physically-based models, each of which has its advantages and disadvantages (Devatha *et al*., 2015). The models differ in inputs required, complexity, data requirement for soil erosion modeling, relationship between input and output, and validation procedures (Merritt *et al*., 2003; Anejionu *et al*., 2013).

Empirical models are constructed on experimental observations. The frequently employed empirical-related models are Modified Universal Soil Loss Equation (MUSLE) (Willams, 1975), the universal soil loss equation (USLE) (Wischmeier & Smith, 1978), the revised universal soil loss equation (RUSLE) (Renard, 1997), and the Erosion Potential Model (EPM) (Gavrilović, 1962; Gavrilovic, 1972; Gavrilovic, 1988). Conceptual models that combine empirical and physically-based models incorporate detailed catchment information in terms of the sediment-producing factors such as rainfall, runoff, and sediment yield (Chandramohan *et al*., 2015). A typical example of conceptual models is LArge Scale CAtchment Model (LASCAM) (Viney & Sivapalan, 1999). Physically-based models describe processes contributing to the entrainment, transport, and deposition of sediment using mathematical equations of momentum, mass, and energy conservation (Morgan *et al*., 1992; Visser *et al*., 2005). The Water Erosion Prediction Project (WEPP) is one of the most commonly used physical models (Laflen *et al*., 1991).

Among these types of soil erosion models, empirical models are considered a good solution for soil erosion modeling when data and parameter inputs are poor. The models often rely upon large amounts of input data, varying spatially and temporally (Merritt *et al*., 2003). However most of them integrated geospatial technologies because they allow the acquisition, analysis, and interpretation of spatial and temporal data on variables required to estimate soil erosion (El Jazouli *et al*., 2017; Ahmadi *et al*., 2019; Gianinetto *et al*., 2019). To support land sustainable management and soil conservation, geographic information system (GIS) and remote sensing (RS) techniques are combined with various soil erosion models to evaluate soil loss rates and map soil loss risk (Smith, 1999; Taheri *et al*., 2013; Barbosa *et al*., 2019; El Jazouli *et al*., 2019b). Furthermore, these mathematical models integrated with geospatial methods have inherent limitations and require relatively detailed calibration data. Thus, the field survey methods by identifying and measuring soil erosion indicators are crucial in soil erosion assessment, though they remain costly, laborious, and time-consuming.

Recently, many direct methods have been developed to provide relatively precise soil erosion data for validating erosion models (Barbosa *et al*., 2019). More effective erosion monitoring methods are tracer methods (i.e. ^{137}Cs, ^{210}Pb, and ^{10}Be) (Gaspar *et al*., 2013; Porto *et al*., 2014; Yuan *et al*., 2020), RTK-GPS instruments (Wu & Cheng, 2005; Cheng *et al*., 2007; Zhang *et al*., 2011; Castillo *et al*., 2014), LiDAR and photogrammetry by Drone (Hout *et al*., 2020; Tak *et al*., 2020), and 3D laser scanners (Haubrock *et al*., 2009). In this context, pedometric such as magnetic susceptibility (MS) methods emerged to predict specific soil properties such as soil organic carbon using mass-specific susceptibility at low frequency (Jakšík *et al*., 2016). Based on rapid measurements of magnetic parameters, the MS technique provides an easy and economical method to assess the soil redistribution caused by erosion and deposition. In past years, a number of research work worldwide have employed the MS method in environmental studies and proved the MS performance and effectiveness in characterizing soil erosion on watershed and sloping land (Menshov *et al*., 2018; Barbosa *et al*., 2019; Liu *et al*., 2019; Yue *et al*., 2019; Ayoubi & Dehaghani, 2020; Mosavi *et al*., 2020).

In Morocco, the arid and semiarid climate marked by high annual temperatures, low precipitation, and flash floods makes the country most vulnerable to soil erosion. The soil is also mainly shallow and protected poorly by vegetation cover. According to the International Atomic Energy Agency (IAEA) Office of Public Information and Communication (IAEA, 2016), soil erosion affects over 40 % of Morocco's total land area. It is further compounded by deforestation, overgrazing, and lack of planning strategies. Besides the soil quality and productivity, the huge soil losses in Morocco, with an average annual of over 100 million tonnes that partially reach the dam reservoirs, reduce their water storage capacity. Thus, soil erosion assessment is imperative to identify erosion-prone areas. Most of the studies have been conducted at many Moroccan watersheds in attempting to evaluate the soil erosion rate and risks using various methods (Benmansour *et al*., 2013; Chaaouan *et al*., 2013; Bachaoui *et al*., 2014; Simonneaux *et al*., 2015; Elaloui *et al*., 2017; Ahmed *et al*., 2019; Jazouli *et al*., 2019; Markhi *et al*., 2019; Bou-imajjane *et al*., 2020). These examples of previous studies, among others, employed various methods to estimate the rate of erosion and to map highly vulnerable areas. Field survey, empirical models (USLE, RUSLE, EPM, SWAT…), and radionuclide techniques (^{137}Cs, ^{210}Pbex) combined with a GIS environment are the common approaches used to provide more detailed and reliable data on potential soil loss and sediment yield at a catchment scale.

In this work, we attempt to model the potential rate of soil erosion in the Srou watershed located in the Moroccan Middle by applying Gavrilovic's EPM model integrated with GIS and MS measurements. The EPM model considers lithology (sensibility of soil to erosion), topography, soil protection (vegetation cover), and climatic factors of the catchment, which seem to be the main factors controlling the soil erosion in our mountainous area. The magnetic measurements in a laboratory allow acquiring information about soil properties in top- and subsoil to ensure erosion EPM model validation.

MATERIALS AND METHODS

Study area

The Srou River watershed lies in Khénifra Province in the Middle Atlas Mountain of Morocco (Fig. 1). It is located between 32°34′N - 33°07°N and 5°10′W - 5°50′W (X: 459570 m / 521906 m and Y: 218727 m / 279759 m). It is bordered to the north by the Khénifra city, to the east by Itzer commune, to the south-east by the plain of the upper

Moulouya, and to the west by the Ahmed El Hansali dam. The watershed that extends about 1473 km^2 is drained by the Srou river and its tributaries flowing into the Oum Er Bia River (Fig. 1). The study area is mainly mountainous and highly folded following the early alpine orogeny present topographic variations with elevations ranging from 260 m to 360 m a.s.l. The area geology includes Cretaceous sub-tabular limestone formations, Liasic dolomitic limestones, Triassic doleritic basalts, quartzites, and red clays. The soils derived from these rock outcrops are of different types, including vertisols, calcimagnesic, isohumic, and fersialitic soils (table 1).

Fig. 1: Presentation of study area

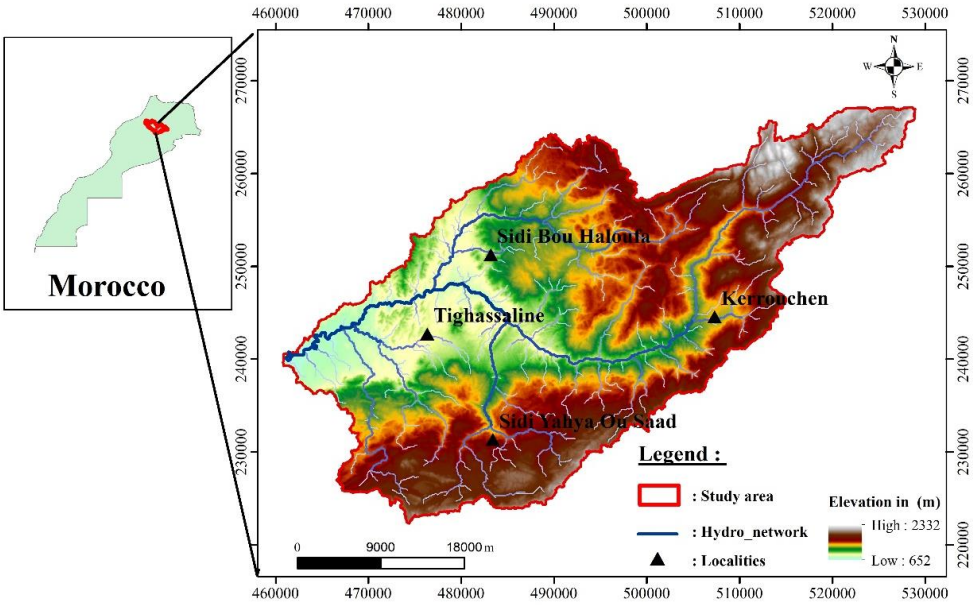

Table 1: Y-factor classes used in this study

Y-factor	Classes	Classe names	Area (km²)	Area (%)
1	0.01-0.10	Soil very resistant to erosion (Vertisols)	703	47.75
2	0.10-0.20	Soil less resistant to erosion (Calcimagnesic soils)	99	6.72
3	0.20-0.37	Soil very sensitive to erosion (Isohumic and Fersialitic soils)	670	45.51

The climatic conditions reflect a warm Mediterranean climate with dry summer, the mean annual temperature is 20.6 °C, and the annual precipitation is 666 mm with peaks in the winter (El Jazouli *et al.*, 2019a). More than 90 % of the rainfall occurs between December to April, with an erosivity of 1444.48 MJ.mm/(ha.h.yr). Agriculture and livestock, especially sheep and goats, are the dominant activities in the region, which control the LULC dynamic. Therefore, these activities linked to population growth increase (1.7 %) lead to the expansion

of agricultural and grazing lands at the expense of the forest in that catchment. The motivation of the present study is to evaluate the combined impact of land use change, geomorphological characteristics, and climate in the Srou watershed (Middle Atlas, Morocco) on soil erosion.

Data collection and processing

The Srou watershed is one of the Moroccan mountainous basins that suffers from soil erosion concerns accentuated by climate changes, landscape, deforestation, pastures, tillage, and lack of land conservation programs. The impact of LULC change on soil erosion is rather limited in the study area. (El Jazouli *et al*., 2019b) modeled soil erosion with changing LULC influences by employing CA-Markov and RUSLE equation. The results obtained are promising, even if the RUSLE model only applies to sheet erosion in areas with a slope not exceeding 20° (Chaaouan *et al*., 2013), which is not the case of the Srou watershed. Therefore, the novelty of the current study is the combination of EPM empirical model with MS measurements in a laboratory. EPM has the potential to estimate erosion and sediment transport in the study watershed because it is suitable for areas with various types of erosion (erosion in sheets, rills, gully erosion, and bank walls). The data related to the climate, topography, soil type, and land use are required for the EPM model to estimate the annual potential soil erosion.

The average annual soil loss (W) is calculated in $m^3\,km^{-2}\,year^{-1}$ using Eq. (1) (Gavrilovic, 1988):

$$W = T.H.\pi.\sqrt{Z^3} \qquad (1)$$

where T is the temperature coefficient, H is the average annual rainfall (mm), $\pi = 3.14$, and Z is the erosion intensity.

The T coefficient is obtained based on Eq. (2) (Gavrilovic, 1988). However, land temperature influences the availability of water in soil and plants and the soil physicochemical properties like structure, texture, and aggregate stability (Arocena & Opio, 2003; Terefe *et al*., 2008; Allison *et al*., 2010; Inbar *et al*., 2014). The spatial annual land temperature was obtained using Landsat 8 OLI images from 2018 and 2019 because the local Weather stations lack temperature data.

$$T = \sqrt{\left(\frac{t^0}{10} + 0,1\right)} \qquad (2)$$

where t^0 is the mean annual temperature (°C)

The coefficient of erosion intensity (Z) representing the quantitative erosion intensity (Staut, 2004) is calculated using Eq. (3) :

$$Z = Xa.Y.\psi.\sqrt{S} \qquad (3)$$

where Xa is the soil protection coefficient, Y is the rock and soil sensibility to erosion, Ψ is the erosive state coefficient of the watershed, and S is the coefficient of the slope. According to the Z values, the areas where the high degrees of influence coincide correspond to the areas most vulnerable to erosion and vice versa.

The land cover is considered one of the most important biophysical key factors of soil loss (Rawat & Singh, 2018). Vegetation cover conditions the degree of soil protection represented by the Xa coefficient. Therefore, the land-cover classification was derived using a Landsat 8 OLI image from 24/02/2019 using Normalized Different Vegetation Index (NDVI)

thresholds. NDVI is an indicator widely used to measure plant greenness within satellite data given as Eq. (4) (Tucker, 1979).

$$\boldsymbol{NDVI = \frac{NIR - RED}{NIR + RED}} \qquad \textit{(4)}$$

where, NIR is the reflectance of the near-infrared band (0.85-0.88 μm), and RED is the reflectance of the red band (0.64-0.67 μm).

After the classification based on NDVI values, the XaNDVI value was calculated using the methodology proposed by Chaaouan et al. (2013). The obtained XaNDVI value is used to calculate the Xa factor values according to Eq. (5).

$$\boldsymbol{Xa = (XaNDVI - 0.61) * (-1.25)} \qquad \textit{(5)}$$

Soil granulometry and OM commonly affect the soil water content and, consequently, the amount of runoff (Saxton & Rawls, 2006). EC with high values favor soil erosion by piping processes (Faulkner *et al*., 2004). By the lack of a soil map of Srou river watershed, the Y factor was evaluated from data of (El Jazouli *et al*., 2020) and soil analyses conducted in the present study. Furthermore, the empirical Eq. (6) adapted in the Moroccan case (Merzouk, 1985) was employed to calculate Y factor:

$$\boldsymbol{Y = 311.63 - 4.48(SG\% + S\%) + 613.4 + 6.45\, EC} \qquad \textit{(6)}$$

where, SG is the coarse sand content (%), S is the sand content (%), and EC is the electrical conductivity (ms/cm).

The erosive state coefficient (Ψ-factor) of the watershed that provides information on the state of soil erosion was calculated by using the method based on the Landsat red band (OLI4) as proposed by Zorn & Komac (2009) Eq.(7). This method was used in a semi-arid Moroccan context to draw up the map of the erosive state (Ahmed et al. 2019).

$$\boldsymbol{\Psi = \sqrt{\frac{OLI4}{Q_{max}}}} \qquad \textit{(7)}$$

where, OLI represents the radiance in the red region (0,636 – 0,673 μm), and Qmax is the maximum spectral radiance of OLI4.

The average annual soil loss (W) calculated was then used to estimate the amount of sediment reaching the watershed outlet (G) following Eq. (8):

$$\boldsymbol{G = W.\rho.SDR} \qquad \textit{(8)}$$

where ρ is the density of the sediment and SDR is the delivery coefficient employing the USDA Soil Conservation Service 1972 method (USDA 1972), Eq. (9):

$$\boldsymbol{SDR = 0.4724 * A^{-0,125}} \qquad \textit{(9)}$$

where, A is the area of the watershed in km^2.

To determine the MS vertical evolution in the Srou watershed, 116 samples covering the whole study area were collected along the horizontal transects and from the vertical profiles (at 10cm, 20cm, 30cm and 40cm) while considering the slope for substrate and land use types. For comparison, sampling was carried out along a profile through protected land where the slope is shallow, and the vegetation is dense. At the Srou basin outlet, samples were taken along a vertical profile. This sampling method would allow us to assess the variation of erosion according to these factors. It was also adopted to validate the results of Gavrilovic's ''EPM'' model and determine the source areas of the sediments reaching the

basin outlet. For this reason, a quantity of about 14 g of the sample is compressed in a 10 ml volume vial made for these measurements to avoid particle movement. The vial is placed in a Bartington susceptibility meter with an MS2B probe which creates a magnetic field at two frequencies: low frequency (lf) and high frequency (hf), leading, respectively, to low (Xlf) and high frequency (Xhf) magnetic susceptibilities by applying Eq. (10):

$$\chi = \frac{M}{H} \qquad (10)$$

where, χ is the mass-specific magnetic susceptibility in m^3/kg, and M is the reversible magnetisation per unit mass of the sample placed in the magnetic field H.

Fig. 2: Flow chart of the methodology adopted in this study

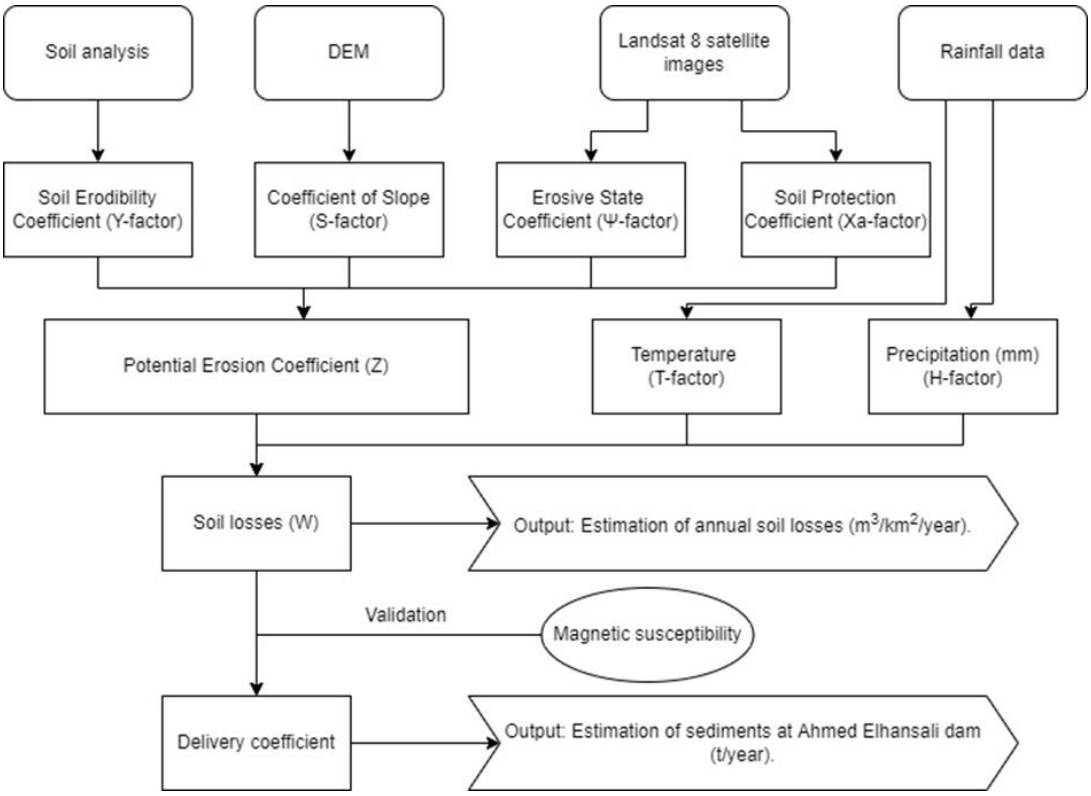

Implementing the EPM model required the GIS application to produce soil erosion intensity maps in the study area. To prepare thematic maps for each EPM parameter, the database taken into consideration are: (1) Landsat 8 OLI images (24-02-2019) with a spatial resolution of 30 m obtained from the U.S. Geological Survey (USGS) (https://glovis.usgs.gov/) for LULC map, normalized difference vegetation index (NDVI), surface temperature, and erosive state coefficient of the watershed, (2) ASTER digital elevation model (DEM) with a spatial resolution of 30 m was used to extract topographic functions (for developing maps of slope), (3) geologic map of Rabat at a scale of 1:500,000 and soil analysis such as the texture and electrical conductivity of the soil (for estimating the

erodibility factor) and precipitation data from ABHOER (for mapping the average annual rainfall). The databases were processed using ArcGis 10.3 and ENVI 5.3 software. The validity of the model was checked about the field data and MS measurement results. Therefore, the field visits were done to verify the nature of soil erosion and collect soil samples for electrical conductivity, texture, iron content, and MS measurements. The EPM model coupled with the GIS software and the MS method were used to conduct the present investigation. A flowchart presented in Fig. 2 depicted the methodology adopted in the present study.

RESULTS AND DISCUSSION

The Gavrilovic's EPM model necessitated the mapping and combining of the different factors required for its operation in a platform of GIS to perform the cell-by-cell calculation of the average annual rate of soil loss ($m^3/km^2/year$) and to identify the source zones of the sediments responsible for the siltation of the Ahmed El Hansali dam using the magnetic susceptibility technique. The EPM model parameters derived from different data sources were developed and discussed.

Temperature (T-factor)

Water erosion is primarily controlled by climate, and temperature and solar radiation are parameters that influence the state of soils on a large scale. The T-coefficient map was created in a GIS environment by applying Eq. (2), showing that the T-coefficient varied between 0.31 and 2.07 °C (Fig. 3, a). Generally, the highest values of the factor (T) are located in the western part of the basin, where vegetation is weak, the slope is low, and soil erodibility increases. It is also noted that this factor is concentrated at the level of watercourses.

Rainfall (H-factor)

Generally, rainfall is the leading cause of soil destruction and degradation and the transport of sediments by runoff (Chaaouan *et al*., 2013). The H-factor refers to the average annual rainfall that is one of the driving forces behind soil erosion. Several annual rainfall data (1968 to 2016) of the surrounding meteorological stations of El Hansali, Lahri and Tamchachat were used to compute the long-term annual rainfall of the study watershed (varying between 500 and 700 mm) and to map the H-factor using the Kriging techniques within the ArcGIS environment (Fig. 3b). A clear increase in average rainfall as a function of altitude and from downstream to upstream from the watershed was observed.

Fig. 3: (a), T-factor (T) map of the study area; (b), H-factor (H) map of the study area; (c), Xa -factor map of the study area; (d), Map of the soil sensitivity factor to erosion in the study area; (e), Ψ-factor map of the study area; (f), Map of the slope factor of the study area.

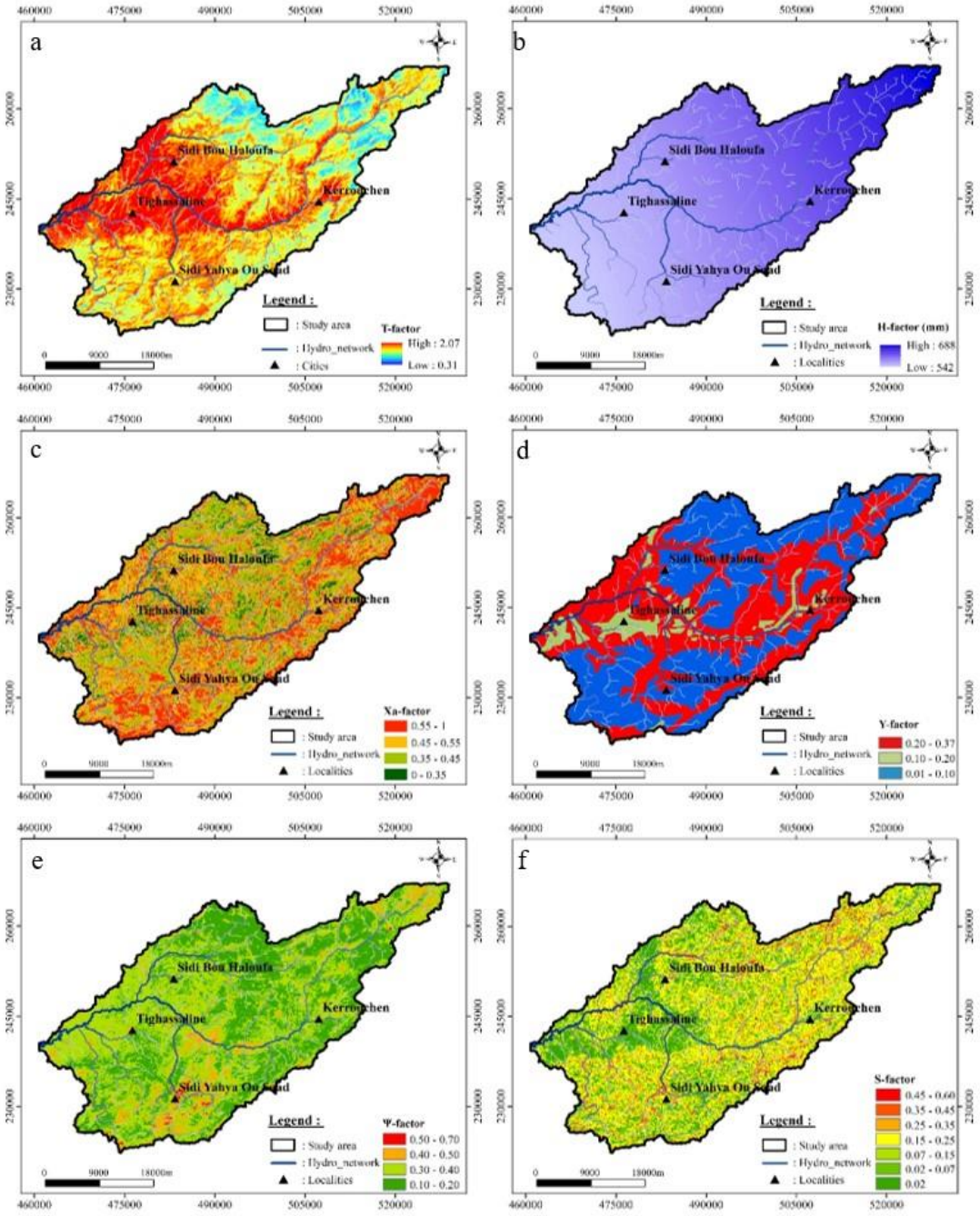

Soil protection factor (Xa-factor)

As shown in Fig. 3c and Table 2, four major land cover types have been distinguished. Class 1, ranging between 0.02 and 0.35 and representing areas with very dense vegetation, concerned 6.13 % of the total catchment area. Class 2, with values between 0.35 and 0.45, corresponded to areas covered by sparse vegetation. Class 3, having values varying between 0.45 and 0.55, represented damaged cultivated land over an area of around 39.48 %. Class 4 between 0.55 and 1, corresponded to land without vegetation.

Table 2: Xa-factor classes used in this study

Xa-factor	Classes	Classe names	Area (km²)	Area (%)
1	0.00-0.35	Areas where the vegetation is very dense.	90.26	6.13
2	0.35-0.45	Areas covered by spaced plants.	401.02	27.24
3	0.45-0.55	Damaged pasture and cultivated land.	581.08	39.48
4	0.55-1	Areas without vegetal cover.	399.40	27.13

Soil sensitivity to erosion factor (Y-factor)

The Y-factor reflects the proportion of soil particles detached and carried by rainfall-runoff, and it expresses the resistance degree of soil to the erosive force of rainfall. Among the soil properties that affect soil erodibility, the soil texture, OM content, and EC largely contribute to the control of vulnerability to erosion and capability of sediment production.

The Y value of soils in the study watershed classified into three classes varied from 0.01 (low erodibility) and 0.37 (strong erodibility). The first class represents 47.75 %, the second class represents 6.72 %, and the last class concerns 45.51 % of the total surface of the watershed (Table. 1; Fig. 3, d).

Erosive state factor (Ψ-factor)

The Ψ-factor of the study area is classified into four categories (Table. 3; Fig. 3, e). It generally ranged from 0.18 to 0.66, indicating erosion principally in waterways on 20–50 % of the catchment area and secondary in rivers, gullies, alluvial deposits, and karst.

Table 3: Ψ-factor classes used according to the classification of Gavrilovic 1988

Ψ-factor	Classes	Classe names	Area (km²)	Area (%)
1	0.10-0.20	Little erosion on watershed	574.02	38.94
2	0.30-0.40	Erosion in waterways on 20-50% of the catchment area	111.41	7.55
3	0.40-0.50	Erosion in rivers, gullies and alluvial deposits, karstic erosion	781.46	53.02
4	0.50-0.70	50-80% of catchment area affected by surface erosion and landslides	6.08	0.41

Slope of the watershed (S-factor)

The landform shape is a major factor influencing soil erosion because it controls soil and vegetation development and surface runoff. Its effect on soil erosion in the EPM model is performed by S-factor, the product of slope steepness, derived in this study from a DEM with a resolution of 30 m of the Srou watershed through Raster Surface tools in ArcGIS.

According to Gavrilovic (1988), the slope map of the study watershed is classified into seven classes, each of which corresponds to a specific the S-factor (Table. 4). The majority (about 86.38 %) of the slope percentage is <30 % in the western part of the study area, generally coinciding with areas of low altitude, whereas about 14 % of the slope is over 30 % and is scattered throughout the study area (Fig. 3, f).

Table 4: S-factor classes used according to the classification of Gavrilovic 1988

Slope factor (S)	Classes	Slope (%)	Area (km²)	Area (%)
1	0-0.02	0-5	351.96	23.89
2	0.02-0.07	5-10	404.29	27.44
3	0.07-0.15	10-20	306.26	20.79
4	0.15-0.25	20-30	210.10	14.26
5	0.25-0.35	30-40	126.30	8.57
6	0.35-0.45	40-50	58.56	3.97
7	0.45-0.60	>50	15.46	1.04

Potential erosion coefficient (Z)

The potential erosion parameter (Z) makes it possible to hierarchize the surface of a watershed into units distinguished according to the vulnerability to erosion. It is based on a thematic mapping of erosion factors such as soil protection factor, soil sensibility to erosion factor, erosive state factor, and slope. The superposition of these maps results in a potential erosion map in which the areas where the high degrees correspond to the area most vulnerable to erosion (Fig. 4a).

Fig. 4: (a), Potential erosion coefficient (Z) map; (b), Annual average soil loss map of Oued Srou watershed by EPM.

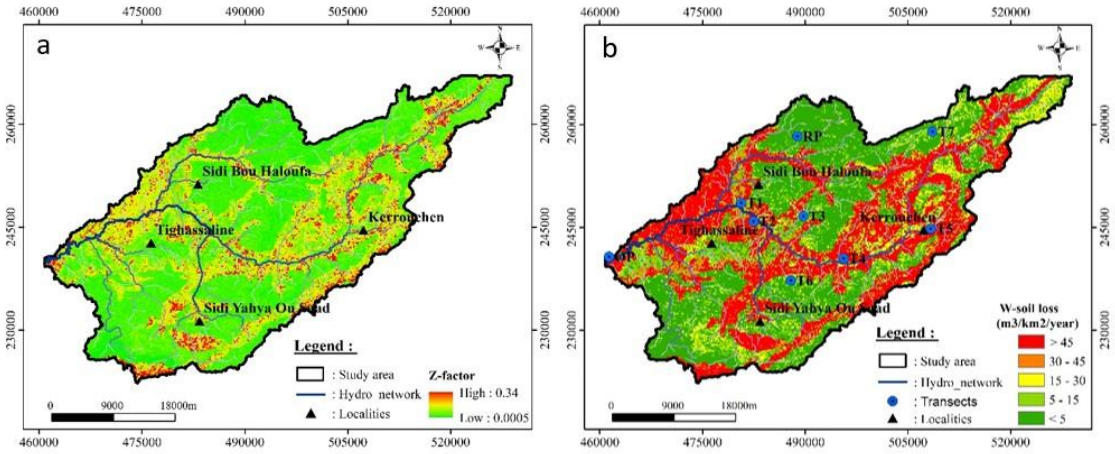

Annual soil erosion estimation (W)

The erosion risks assessment in the Srou watershed was performed by multiplying the input EPM factor maps using a GIS environment. The risk map of water erosion of soils in the Srou watershed is classified into five classes according to the classification proposed by Al Karkouri (2003): very low (< 5 m^3/km^2/year), low erosion (5-15 m^3/km^2/year), moderate erosion (15-30 m^3/km^2/year), high erosion, and very high erosion (>45 m^3/km^2/year) affecting 35.46 %, 15.57 %, 6.85 %, 4.67 %, and 36.61 % of the total catchment area, respectively (Table 5). As shown in the soil erosion map (Fig. 4b), the highest values of estimated soil erosion occurred in the mainstream due to their high Y-factor values. The minimum soil losses with values less than 5 m^3/km^2/year are generally in highly protected areas with dense vegetation. However, the total annual soil losses in the whole catchment area are about 194288 t/year, means that a large part of these sediments reaches the Ahmed El Hansali dam. Our results are quite similar to those of other previous works on the Oued Srou watershed (Elbouqdaoui *et al*., 2005), showing that the very high and extremely high risk of erosion concerned 35.5 % of the total watershed areas. Jihad (2010) reported that the specific soil degradation in the Srou River could reach 3000 t/km^2/year on clay soils. (Mohamed, 2021) showed, based on the EPM model at the level of the Tagueleft watershed in the Central High Atlas, that the rate of soil loss due to water erosion varied at the basin scale between 0.71 m^3/km^2/year, as the minimum rate in areas very resistant and well protected by forest cover, and a higher rate (17000 m^3/km^2/year) corresponding to the linear and concentrated and spreading erosion affecting areas with steep slopes and no vegetation. Gavrilovic's EPM model remains the most reliable model for estimating soil loss by water erosion in rugged mountain environments.

Table 5: Soil loss in the Srou basin according to the classification proposed by Alkarkouri (2003)

Annual soil loss (W)	Classes	Classe names	Area (km^2)	Area (%)
1	< 5	Very low erosion	526.28	35.46
2	5-15	Low erosion	231.07	15.57
3	15-30	Moderate erosion	101.71	6.85
4	30-45	High erosion	69.31	4.67
5	> 45	Very high erosion	528.58	36.61

Delivery coefficient

The EPM model and spatial analysis techniques show that about 73000 m^3/year of the sediments have been mobilized by water erosion, which would allow us to say that a quantity of these sediments reaches the Ahmed El Hansali Dam. The delivery coefficient showed that about 34433 t/year of sediment reached the watershed outlet. Therefore, it is urgent to reduce the quantities of material lost through erosion that end up in the watercourses and the Ahmed El Hansali dam by developing and revegetating the Oued Srou watershed.

Correlation

The matrix correlation based on the Pearson coefficient (R2) was computed to examine the mutual relationships between the input parameters and determine their importance degree in the Srou watershed. The correlation results (Table 6) revealed that soil sensibility to erosion is similarly the most decisive factor in erosive dynamics with R^2 of about 0.58, followed by the soil protection factor with R^2 of 0.37, the slope factor with R^2 of 0.19, the erosive state with R^2 of 0.17, the T-factor with a correlation coefficient of 0.16. Finally, the precipitation factor correlates weakly with soil losses at 0.04. The sensibility of soil to erosion is even more related to the temperature factor with R^2 of about 0.30.

Table 6: Correlation matrix between the input factors of the EPM model

Input factors	W	Y	Xa	S	Phi	H	T
Soil loss (W)	**1**	0.58	0.37	0.19	0.17	0.04	0.16
Y-factor	0.58	**1**	0.002	0.01	0.07	-0.05	0.30
Xa-factor	0.37	0.002	**1**	0.02	0.25	0.07	0.04
S-factor	0.19	0.01	0.02	**1**	-0.13	0.24	-0.23
Ψ-factor	0.17	0.07	0.25	-0.13	**1**	-0.24	0.41
H-factor	0.04	-0.05	0.07	0.24	-0.24	**1**	-0.43
T-factor	0.16	0.30	0.04	-0.23	0.41	-0.43	**1**

Validation

We used the magnetic susceptibility technique to evaluate the results of the empirical EPM model by assessing the response of samples collected at low frequency. It was established in the late 1970s that soil particle magnetic susceptibility might be used for environmental applications such as predicting sediment supply locations (Thompson *et al*., 1975). Le Borgne (1955) was the first to observe the phenomenon of increasing magnetic susceptibility of soil particles from the parental material to the surface of developed soil. The locations of all transects (P1 = upslope & P4 = downslope) were defined according to the major factors controlling erosion, namely slope, substrate type, and land use. Table 7 shows the lithological and land use characteristics and the average MS of samples from all transects.

The response of low-frequency MS along soil transects provided essential information on the state of soil degradation. It highlighted several fundamental points on soil stability in the Srou watershed: the substrate influenced the soil ferromagnetic mineral content, and the plant cover allows better soil protection. Uneroded soils showed a normal increasing MS trend from the bedrock to the surface. The MS vertical evolution from the bedrock to the surface is disturbed for eroded soils.

Table 7: Substrate types, land cover and magnetic susceptibility of transects

Transects	T1	T2	T3	T4	T5	T6	T7	P-R	P-Outlet
Lithology	Silty clays	Clay	Basalt and clay	Limestone and clay	Clay and sandstones	Limestone and clay	Limestone and clay	Clay and limestone	River terrace
Plant cover	Spaced plants	Forest	Trees, wheat and grass	Ploughed wheat and fallow land	Grass	wheat	No vegetation cover	Dense forest	No vegetation cover
χ_{LF} **mean** (10^{-8} m^3/kg)	53.80	113.00	565.00	351.00	10.40	29.60	120.00	236.00	91.80
χ_{LF} **min** (10^{-8} m^3/kg)	6.92	7.99	157.02	10.55	5.85	16.74	7.80	139.55	81.48
χ_{LF} **max** (10^{-8} m^3/kg)	278.36	336.94	836.99	738.79	25.62	41.31	286.10	353.56	109.29

The analyses of results of low-frequency MS would allow us to conclude the following points (Figs. 5 and 6):

- Transect 1 (silty clays & sparse vegetation): the four profiles show two trends in the MS evolution. Profile 1 shows low MS values for depths greater than 20 cm with a sharp increase towards the surface, characterizing an evolved soil. A very weak evolution of the magnetic susceptibility from the bedrock to the surface is observed for the other profiles. This indicates an intense erosion with a colluviation towards profile 2, showing an MS increase towards the 10 cm of the surface.
- Transect 2 (clay & forest): shows a clear change in MS compared to the first transect. The first profile (upslope) showed a normal evolution of the susceptibility except for the sample 10 cm; this would allow us to say that part of the sediments is eroded followed by a deposition towards the last low slope profile marked by an increase in magnetic susceptibility.
- Transect 3 (Basalt & clay & vegetation cover): the low-frequency MS measured on basalts shows high values compared to clay soil. This increase in susceptibility is mainly due to the magnetic minerals making up basalt. The second profile is also characterized by high MS due mainly to a deposit of the eroded sediments on the basaltic substrate, of which the magnetic susceptibility is increased.
- Transect 4 (limestone & clay & crop): this transect shows an irregular evolution of the magnetic susceptibility values at low frequency. There is a net MS change for the first profile compared to the other profiles. Therefore, the ploughing has probably mixed the soil and its magnetic minerals over the 30 upper cm of the profiles. It suggests that high MS values mark a quantity of the sediments deposited towards the last three profiles.
- Transect 5 (sandstone & clay & grass): This transect shows very low MS values compared to the other transects. These values are either related to the type of substrate depleted in ferromagnetic minerals or related to intense erosion. The first three profiles indicate that this area is undergoing significant erosion marked by low evolution of magnetic susceptibility values.
- Transect 6 (limestone & clay & wheat) and 7 (limestone & clay & bare soil): For these transects with the same type of substrate, the magnetic susceptibility is almost equal for all profiles except for profile T7_P4. The progressive MS evolution suggests that this

zone is undergoing erosion marked by low values and irregular evolution of the magnetic susceptibility. The MS in the fourth profile is due to upstream colluviation followed by downstream deposition.

Fig. 5:Vertical evolution of the MS of the transects T1, T2, T3 and T4 in the Srou watershed

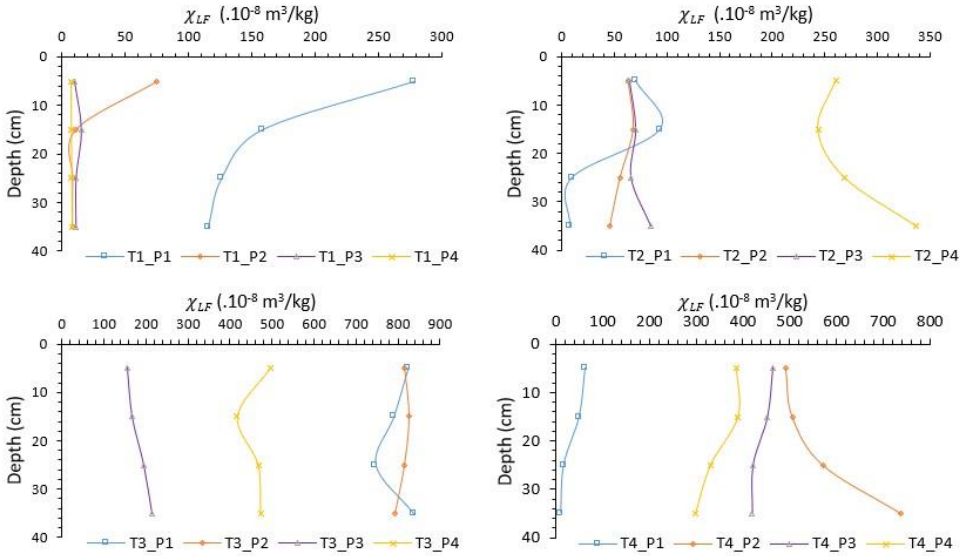

Fig. 6 :Vertical evolution of the MS of the transects T5, T6, T7, Reference profile (RP) and Outlet profile (OP) in the Srou watershed

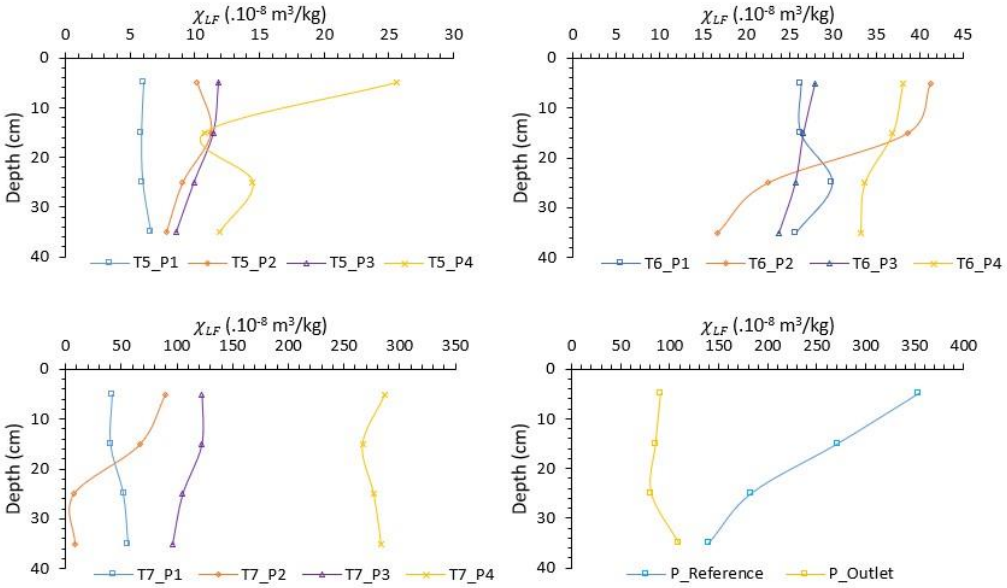

The comparison of MS values at 40 cm depth of the profile at the basin outlet provided information on the sediment origin. The low-frequency MS responses of the outlet profile (OP) are similar to those of transect 2 taken from the Middle Lias clay, suggesting that some of these sediments are reaching the outlet of the basin. The analysis of the normal evolution of the low-frequency MS of the reference site (RP) allowed us to assume that the reference site is located in an area that is not undergoing erosion.

CONCLUSION

The present study aimed to assess soil erosion and sediment yield in the Srou River basin using the empirical EPM model integrated with GIS techniques and MS method. The results showed that the very low, low, medium, high, and very high risks covered about 35, 15, 6, 4, and 36 % of the Srou basin, respectively. The quantity of sediment reaching the river outlet estimated based on the delivery coefficient was about ≃34433 t/year. Our analysis also revealed that the causal factors controlling water erosion in the Srou basin followed the descending order in terms of importance: sensibility of soil to erosion, soil protection, slope, erosive state, temperature, and rainfall. Magnetic susceptibility has allowed us to highlight the source areas of the sediments that reach the Ahmed El Hansali dam. The sediments from the dam came from the area of transect 2 was sampled, as their magnetic susceptibilities are almost similar. From the overall results, the proposed techniques can play a crucial role in controlling soil erosion.

CONFLICT OF INTEREST

The authors declare that they have no competing interests.

REFERENCES

Ahmadi, M., M. Minaei, O. Ebrahimi and M. Nikseresht (2019). *Evaluation of WEPP and EPM for improved predictions of soil erosion in mountainous watersheds: A case study of Kangir River basin*, Iran.

Ahmed, A., D. Adil, B. Hasna, A. Elbachir and R. Lazaar (2019). Using EPM model and GIS for estimation of soil erosion in Souss Basin, Morocco.*Turkish Journal of Agriculture-Food Science and Technology* 7(8): 1228-1232.

Al Karkouri, J. (2003). *Degradation of the natural environment in the Beni Boufrah basin (Central Rif Morocco): analysis of factors and processes, quantification test and spatial modelling.* State doctoral thesis Mohammed V University, Faculty of Letters, Rabat

Allison, S. D., M. D. Wallenstein and M. A. Bradford (2010). Soil-carbon response to warming dependent on microbial physiology. *Nature Geoscience* 3(5): 336-340 DOI: 10.1038/ngeo846.

Anejionu, O. C., P. C. Nwilo and E. S. Ebinne (2013). *Long Term Assessment and Mapping of Erosion Hotspots in South East Nigeria.* FIG Working Week.

Arocena, J. M. and C. Opio (2003). Prescribed fire-induced changes in properties of sub-boreal forest soils. *Geoderma* 113(1): 1-16 DOI: https://doi.org/10.1016 /S0016-7061(02)00312-9.

Ayoubi, S. and S. M. Dehaghani (2020). Identifying impacts of land use change on soil redistribution at different slope positions using magnetic susceptibility. *Arabian Journal of Geosciences* 13: 426.

Bachaoui, B., E. M. Bachaoui, S. Maimouni, R. Lhissou, A. El Harti and A. El Ghmari (2014). The use of spectral and geomorphometric data for water erosion mapping in El Ksiba region in the central High Atlas Mountains of Morocco. *Applied Geomatics* 6(3): 159-169.

Barbosa, R. S., J. M. Júnior, V. Barrón, M. V. Martins Filho, D. S. Siqueira, R. G. Peluco, L. A. Camargo and L. S. Silva (2019). Prediction and mapping of erodibility factors (USLE and WEPP) by magnetic susceptibility in basalt-derived soils in northeastern São Paulo state, Brazil. *Environmental earth sciences* 78(1): 12.

Batista, P. V. G., J. Davies, M. L. N. Silva and J. N. Quinton (2019). On the evaluation of soil erosion models: Are we doing enough? *Earth-Science Reviews* 197: 102898 DOI: https://doi.org/10.1016/j.earscirev.2019.102898.

Benmansour, M., L. Mabit, A. Nouira, R. Moussadek, H. Bouksirate, M. Duchemin and A. Benkdad (2013). Assessment of soil erosion and deposition rates in a Moroccan agricultural field using fallout 137Cs and 210Pbex. *Journal of Environmental Radioactivity* 115: 97-106 DOI: https://doi.org/10.1016/j.jenvrad.2012.07.013.

Borrelli, P., D. A. Robinson, P. Panagos, E. Lugato, J. E. Yang, C. Alewell, D. Wuepper, L. Montanarella and C. Ballabio (2020). Land use and climate change impacts on global soil erosion by water (2015-2070). *Proceedings of the National Academy of Sciences* 117(36): 21994-22001.

Bou-imajjane, L., M. A. Belfoul, R. Elkadiri and M. Stokes (2020). Soil erosion assessment in a semi-arid environment: a case study from the Argana Corridor, Morocco. *Environmental Earth Sciences* 79(18): 409 DOI: 10.1007/s12665-020-09127-8.

Castillo, C., E. V. Taguas, P. Zarco-Tejada, M. R. James and J. A. Gómez (2014). The normalized topographic method: an automated procedure for gully mapping using GIS. *Earth Surface Processes and Landforms* 39(15): 2002-2015.

Chaaouan, J., A. Faleh, A. Sadiki and H. Mesrar (2013). Remote sensing, GIS and modeling of water erosion in the Amzaz River watershed, Central Rif. *French Journal of Photogrammetry and Remote Sensing* (203): 19-25

Chandramohan, T., B. Venkatesh and A. Balchand (2015). Evaluation of three soil erosion models for small watersheds. *Aquatic Procedia* 4: 1227-1234.

Cheng, H., X. Zou, Y. Wu, C. Zhang, Q. Zheng and Z. Jiang (2007). Morphology parameters of ephemeral gully in characteristics hillslopes on the Loess Plateau of China. *Soil and Tillage Research* 94(1): 4-14.

de Jong, E., P. A. Nestor and D. J. Pennock (1998). The use of magnetic susceptibility to measure long-term soil redistribution. *Catena* 32(1): 23-35 DOI: https://doi.org/10.1016/S0341-8162(97)00051-9.

Devatha, C., V. Deshpande and M. Renukaprasad (2015). Estimation of soil loss using USLE model for Kulhan Watershed, Chattisgarh-A case study. *Aquatic Procedia* 4: 1429-1436.

Duan, X., B. Liu, Z. Gu, L. Rong and D. Feng (2016). Quantifying soil erosion effects on soil productivity in the dry-hot valley, southwestern China. *Environmental Earth Sciences* 75(16): 1164 DOI: 10.1007/s12665-016-5986-6.

El Jazouli, A., A. Barakat, A. Ghafiri, S. El Moutaki, A. Ettaqy and R. Khellouk (2017). Soil erosion modeled with USLE, GIS, and remote sensing: a case study of Ikkour watershed in Middle Atlas (Morocco). *Geoscience Letters* 4(1): 1-12.

El Jazouli, A., A. Barakat and R. Khellouk (2019a). GIS-multicriteria evaluation using AHP for landslide susceptibility mapping in Oum Er Rbia high basin (Morocco). *Geoenvironmental Disasters* 6(1): 1-12.

El Jazouli, A., A. Barakat and R. Khellouk (2020). Geotechnical studies for Landslide susceptibility in the high basin of the Oum Er Rbia river (Morocco). *Geology, Ecology, and Landscapes:* 1-8.

El Jazouli, A., A. Barakat, R. Khellouk, J. Rais and M. El Baghdadi (2019b). Remote sensing and GIS techniques for prediction of land use land cover change effects on soil erosion in the high basin of the Oum Er Rbia River (Morocco). R*emote Sensing Applications: Society and Environment* 13: 361-374.

Elaloui, A., C. Marrakchi, A. Fekri, S. Maimouni and M. Aradi (2017). USLE-based assessment of soil erosion by water in the watershed upstream Tessaoute (Central High Atlas, Morocco). *Modeling Earth Systems and Environment* 3(3): 873-885 DOI: 10.1007/s40808-017-0340-x.

Elbouqdaoui, K., H. Ezzine, M. Badrahoui, M. Rouchdi, M. Zahraoui and A. Ozer (2005). Methodological approach by remote sensing and GIS of the evaluation of the potential erosion risk by water in the Srou River watershed (Middle Atlas, Morocco). *Geo-Eco-Trop* 29(1-2): 25-36.

Fang, H. and Z. Fan (2020). Assessment of Soil Erosion at Multiple Spatial Scales Following Land Use Changes in 1980–2017 in the Black Soil Region,(NE) China. I*nternational Journal of Environmental Research and Public Health* 17(20): 7378.

Faulkner, H., R. Alexander, R. Teeuw and P. Zukowskyj (2004). Variations in soil dispersivity across a gully head displaying shallow sub-surface pipes, and the role of shallow pipes in rill initiation. *Earth Surface Processes and Landforms: the Journal of the British Geomorphological Research Group* 29(9): 1143-1160.

Gaspar, L., A. Navas, D. Walling, J. Machín and J. G. Arozamena (2013). Using 137Cs and 210Pbex to assess soil redistribution on slopes at different temporal scales. *Catena* 102: 46-54.

Gavrilovic, S. (1972). *Inzenjering o bujicnim tokovima i eroziji*. Izgradnja. Beograd.

Gavrilović, S. (1962). Proračun srednje-godišnje količine nanosa prema potencijalu erozije (A method for estimating of the average annual quantity of sediments according to the potency of erosion). *Glasnik šumarskog fakulteta* 26: 151-168.

Gavrilovic, Z. (1988). *Use of an Empirical Method (Erosion Potential Method) for Calculating Sediment Production and Transportation in Unstudied or Torrential Streams*. International Conference on River Regime. Hydraulics Research Limited, Wallingford, Oxon UK. 1988. p 411-422, 5 fig, 4 tab, 8 ref.

Gianinetto, M., M. Aiello, F. Polinelli, F. Frassy, M. C. Rulli, G. Ravazzani, D. Bocchiola, D. D. Chiarelli, A. Soncini and R. Vezzoli (2019). D-RUSLE: A dynamic model to estimate potential soil erosion with satellite time series in the Italian Alps. *European Journal of Remote Sensing* 52 (sup4): 34-53.

Haubrock, S.-N., M. Kuhnert, S. Chabrillat, A. Güntner and H. Kaufmann (2009). Spatiotemporal variations of soil surface roughness from in-situ laser scanning. *Catena* 79(2): 128-139.

Hou, X., J. Shao, X. Chen, J. Li and J. Lu (2020). Changes in the soil erosion status in the middle and lower reaches of the Yangtze River basin from 2001 to 2014 and the impacts of erosion on the water quality of lakes and reservoirs. *International Journal of Remote Sensing* 41(8): 3175-3196 DOI: 10.1080/01431161.2019.1699974.

Hout, R., V. Maleval, G. Mahe, E. Rouvellac, R. Crouzevialle and F. Cerbelaud (2020). UAV and LiDAR Data in the Service of Bank Gully Erosion Measurement in Rambla de Algeciras Lakeshore. *Water* 12(10): 2748.

IAEA (The International Atomic Energy Agency) (2016). *Erosion in Moroccan Watersheds Can Be Reduced up to 60 Percent Through the Use of Isotopic Techniques*. Retrieved April, 2nd, 2021 from https://urlz.fr/hSCG, page consulted on 02/04/2022.

Inbar, A., M. Lado, M. Sternberg, H. Tenau and M. Ben-Hur (2014). Forest fire effects on soil chemical and physicochemical properties, infiltration, runoff, and erosion in a semiarid Mediterranean region. *Geoderma* 221-222: 131-138 DOI: https://doi.org/10.1016/j.geoderma.2014.01.015.

Issaka, S. and M. A. Ashraf (2017). Impact of soil erosion and degradation on water quality: a review. *Geology, Ecology, and Landscapes* 1(1): 1-11 DOI: 10.1080/24749508.2017.1301053.

Jakšík, O., R. Kodešová, A. Kapička, A. Klement, M. Fer and A. Nikodem (2016). Using magnetic susceptibility mapping for assessing soil degradation due to water erosion. *Soil and Water Research* 11(2): 105-113.

Jazouli, A. E., A. Barakat, R. Khellouk, J. Rais and M. E. Baghdadi (2019). Remote sensing and GIS techniques for prediction of land use land cover change effects on soil erosion in the high basin of the Oum Er Rbia River (Morocco). *Remote Sensing Applications: Society and Environment* 13: 361-374 DOI: https://doi.org/10.1016/j.rsase.2018.12.004.

Jihad, M.-D. E. (2010). Difficulties in natural resources managing and rural development in an anthropized environment: Experience of the Oued Srou Project (central Morocco). Norois. *Environment, planning, society* (216): 25-45.

Ketema, A. and G. S. Dwarakish (2019). Water erosion assessment methods: a review. *ISH Journal of Hydraulic Engineering:* 1-8 DOI: 10.1080/09715010.2019.1567398.

Kinnell, P. I. A. (2017). A comparison of the abilities of the USLE-M, RUSLE2 and WEPP to model event erosion from bare fallow areas. *Science of The Total Environment* 596-597: 32-42 DOI: https://doi.org/10.1016/j.scitotenv.2017.04.046.

Laflen, J. M., L. J. Lane and G. R. Foster (1991). WEPP: A new generation of erosion prediction technology. *Journal of Soil and Water Conservation* 46(1): 34-38.

Lal, R. (2003). Soil erosion and the global carbon budget. *Environment international* 29(4): 437-450.

Lal, R., D. Mokma and B. Lowery (1999). Relation between soil quality and erosion. *Soil quality and soil erosion* 4: 237-258.

Le Borgne, E. (1955). Abnormal magnetic susceptibility of the surface soil. *Ann. Geophys.*: 399-419.

Liu, L., K. Zhang, S. Fu, B. Liu, M. Huang, Z. Zhang, F. Zhang and Y. Yu (2019). Rapid magnetic susceptibility measurement for obtaining superficial soil layer thickness and its erosion monitoring implications. *Geoderma* 351: 163-173.

Luetzenburg, G., M. J. Bittner, A. Calsamiglia, C. S. Renschler, J. Estrany and R. Poeppl (2020). Climate and land use change effects on soil erosion in two small agricultural catchment systems Fugnitz–Austria, Can Revull–Spain. *Science of The Total Environment* 704: 135389.

Markhi, A., N. Laftouhi, Y. Grusson and A. Soulaimani (2019). Assessment of potential soil erosion and sediment yield in the semi-arid N′fis basin (High Atlas, Morocco) using the SWAT model. *Acta Geophysica* 67(1): 263-272 DOI: 10.1007/s11600-019-00251-z.

Martín-Moreno, C., J. F. Martín Duque, J. M. Nicolau Ibarra, N. Hernando Rodríguez, M. Á. Sanz Santos and L. Sánchez Castillo (2016). Effects of Topography and Surface Soil Cover on Erosion for Mining Reclamation: The Experimental Spoil Heap at El Machorro Mine (Central Spain). *Land Degradation & Development* 27(2): 145-159 DOI: https://doi.org/10.1002/ldr.2232.

Menshov, O., O. Kruglov, S. Vyzhva, P. Nazarok, P. Pereira and T. Pastushenko (2018). Magnetic methods in tracing soil erosion, Kharkov Region, Ukraine. *Studia Geophysica et Geodaetica* 62(4): 681-696.

Merritt, W. S., R. A. Letcher and A. J. Jakeman (2003). A review of erosion and sediment transport models. *Environmental Modelling & Software* 18(8-9): 761-799.

Merzouk, A. (1985). *Relative erodibility of nine selected Moroccan soils related to their physical and chemical and mineralogical properties*, Ph-D Thesis, University of Minnesota, USA.

Mohamed, R. (2021). *The Risk of Water Erosion on the Foothills of the Middle High Atlas (Morocco)*. Tagueleft Basin Case Study.

Mohammed, S., A. Al-Ebraheem, I. J. Holb, K. Alsafadi, M. Dikkeh, Q. B. Pham, N. T. T. Linh and S. Szabo (2020). Soil management effects on soil water erosion and runoff in central Syria—A comparative evaluation of general linear model and random forest regression. *Water* 12(9): 2529.

Morgan, R., J. Quinton and R. Rickson (1992). *EUROSEM documentation manual*. Silsoe College, Silsoe, Bedford, UK: 34.

Mosavi, A., F. Sajedi-Hosseini, B. Choubin, F. Taromideh, G. Rahi and A. A. Dineva (2020). Susceptibility mapping of soil water erosion using machine learning models. *Water* 12(7): 1995.

Novara, A., A. Pisciotta, M. Minacapilli, A. Maltese, F. Capodici, A. Cerdà and L. Gristina (2018). The impact of soil erosion on soil fertility and vine vigor. A multidisciplinary approach based on field, laboratory and remote sensing approaches. *Science of The Total Environment* 622-623: 474-480 DOI: https://doi.org/10.1016/j.scitotenv.2017.11.272.

Panagos, P. and A. Katsoyiannis (2019). *Soil erosion modelling: The new challenges as the result of policy developments in Europe*, Elsevier.

Plambeck, N. O. (2020). Reassessment of the potential risk of soil erosion by water on agricultural land in Germany: Setting the stage for site-appropriate decision-making in soil and water resources management. *Ecological Indicators* 118: 106732.

Porto, P., D. E. Walling and A. Capra (2014). Using 137Cs and 210Pbex measurements and conventional surveys to investigate the relative contributions of interrill/rill and gully erosion to soil loss from a small cultivated catchment in Sicily. *Soil and Tillage Research* 135: 18-27.

Rãdoane, M. and N. Rãdoane (2005). Dams, sediment sources and reservoir silting in Romania. *Geomorphology* 71(1): 112-125 DOI: https://doi.org/10.1016/j.geomorph.2004.04.010.

Rawat, K. S. and S. K. Singh (2018). Appraisal of Soil Conservation Capacity Using NDVI Model-Based C Factor of RUSLE Model for a Semi Arid Ungauged Watershed: a Case Study. *Water Conservation Science and Engineering* 3(1): 47-58 DOI: 10.1007/s41101-018-0042-x.

Renard, K. G. (1997). *Predicting soil erosion by water: a guide to conservation planning with the Revised Universal Soil Loss Equation (RUSLE)*, United States Government Printing.

Rozos, D., H. D. Skilodimou, C. Loupasakis and G. D. Bathrellos (2013). Application of the revised universal soil loss equation model on landslide prevention. An example from N. Euboea (Evia) Island, Greece. *Environmental Earth Sciences* 70(7): 3255-3266.

Saxton, K. E. and W. J. Rawls (2006). Soil water characteristic estimates by texture and organic matter for hydrologic solutions. *Soil science society of America Journal* 70(5): 1569-1578.

Senanayake, S., B. Pradhan, A. Huete and J. Brennan (2020). A Review on Assessing and Mapping Soil Erosion Hazard Using Geo-Informatics Technology for Farming System Management. *Remote Sensing* 12(24): 4063.

Simonneaux, V., A. Cheggour, C. Deschamps, F. Mouillot, O. Cerdan and Y. Le Bissonnais (2015). Land use and climate change effects on soil erosion in a semi-arid mountainous watershed (High Atlas, Morocco). *Journal of Arid Environments* 122: 64-75 DOI: https://doi.org/10.1016/j.jaridenv.2015.06.002.

Smith, H. (1999). Application of empirical soil loss models in southern Africa: A review. *South African Journal of Plant and Soil* 16(3): 158-163.

Staut, M. (2004). *Recent erosional processes in the catchment of the Dragonja river*. Unpublished graduate thesis. Faculty of Arts, University of Ljubljana, Ljubljana.(In Serbian).

Sthiannopkao, S., S. Takizawa, J. Homewong and W. Wirojanagud (2007). Soil erosion and its impacts on water treatment in the northeastern provinces of Thailand. *Environment International* 33(5): 706-711 DOI: https://doi.org/10.1016/j.envint.2006.12.007.

Taheri, M., A. Landi and B. Archangi (2013). Using Rs, GIS systems and MPSIAC model to produce erosion map and to estimate sedimentation. *International Journal of Agriculture* 3(4): 881.

Tak, W., K. Jun, S. Kim and H. Lee (2020). Using Drone and LiDAR to Assess Coastal Erosion and Shoreline Change due to the Construction of Coastal Structures. *Journal of Coastal Research* 95(SI): 674-678.

Terefe, T., I. Mariscal-Sancho, F. Peregrina and R. Espejo (2008). Influence of heating on various properties of six Mediterranean soils. A laboratory study. *Geoderma* 143(3-4): 273-280 DOI: 10.1016/j.geoderma.2007.11.018.

Thompson, R., R. W. Battarbee, P. O'sullivan and F. Oldfield (1975). Magnetic susceptibility of lake sediments. *Limnology and Oceanography* 20(5): 687-698.

Tucker, C. J. (1979). Red and photographic infrared linear combinations for monitoring vegetation. *Remote sensing of Environment* 8(2): 127-150.

USDA (1972). *Sediment sources, yields, and delivery ratios*. National Engineering Handbook, Section 3 Sedimentation.

Viney, N. R. and M. Sivapalan (1999). A conceptual model of sediment transport: application to the Avon River Basin in Western Australia. *Hydrological Processes* 13(5): 727-743.

Visser, S., G. Sterk and D. Karssenberg (2005). Modelling water erosion in the Sahel: application of a physically based soil erosion model in a gentle sloping environment. *Earth Surface Processes and Landforms: The Journal of the British Geomorphological Research Group* 30(12): 1547-1566.

Walling, D. E. and Q. He (1999). Improved Models for Estimating Soil Erosion Rates from Cesium-137 Measurements. *Journal of Environmental Quality, John Wiley & Sons, Ltd*. 28: 611-622.

Wang, Y., L. Chen, B. Fu and Y. Lü (2014). Check dam sediments: an important indicator of the effects of environmental changes on soil erosion in the Loess Plateau in China. *Environmental Monitoring and Assessment* 186(7): 4275-4287 DOI: 10.1007/s10661-014-3697-6.

Willams, J. (1975). Sediment-yield prediction with universal equation using runoff energy factor. In present and prospective technology for predicting sediment yields and sources: *Proceedings of the Sediment-Yield Workshop* ((pp. 244-252), USDA Sedimentation Laboratory, Oxford, Miss., Nov. 28-30, 1972, Agricultural Research Service, U.S. Dept. of Agriculture, 1975.

Wischmeier, W. H. and D. D. Smith (1978). *Predicting rainfall erosion losses: a guide to conservation planning*, Department of Agriculture, Science and Education Administration.
Wu, Y. and H. Cheng (2005). Monitoring of gully erosion on the Loess Plateau of China using a global positioning system. *Catena* 63(2-3): 154-166.

Yuan, Y., D. Xiong, H. Wu, L. Liu, W. Li, C. L. Chidi, N. M. Dahal and N. Neupane (2020). Using 137 Cs and 210 Pb ex to trace soil erosion rates for a small catchment in the mid-hills of Nepal. *Journal of Soils and Sediments*: 1-16 DOI: 10.1007/s41324-017-0102-x.

Yue, Y., Z. Keli, L. Liang, M. Qianhong and L. Jianyong (2019). Estimating long-term erosion and sedimentation rate on farmland using magnetic susceptibility in northeast China. *Soil and Tillage Research* 187: 41-49.

Zhang, C.-L., S. Yang, X.-H. Pan and J.-Q. Zhang (2011). Estimation of farmland soil wind erosion using RTK GPS measurements and the 137Cs technique: A case study in Kangbao County, Hebei province, northern China. *Soil and Tillage Research* 112(2): 140-148.

Zorn, M. and B. Komac (2009). Response of soil erosion to land use change with particular reference to the last 200 years (Julian Alps, Western Slovenia). *Revista de geomorfologie* 11: 39-47.